Renewable Energy xxx (2014) 1–8

Contents lists available at ScienceDirect

Renewable Energy

journal homepage: www.elsevier.com/locate/renene

Modeling large offshore wind farms under different atmospheric stability regimes with the Park wake model

Alfredo Peña*, Pierre-Elouan Réthoré, Ole Rathmann

DTU Wind Energy, Risø Campus, Technical University of Denmark, Frederiksborgvej 399, 4000 Roskilde, Denmark

ARTICLE INFO

Article history:
Received 6 September 2013
Accepted 3 February 2014
Available online xxx

Keywords:
Atmospheric stability
Park wake model
Offshore
Wake decay coefficient
WAsP

ABSTRACT

We evaluate a modified version of the Park wake model against power data from a west-east row in the middle of the Horns Rev I offshore wind farm. The evaluation is performed on data classified in four different atmospheric stability conditions, for a narrow wind speed range, and a wide range of westerly wind directions observed at the wind farm. Simulations (post-processed to partly account for the wind direction uncertainty) and observations show good agreement for all stability classes, being the simulations using a stability-dependent wake decay coefficient closer to the data for the last turbines on the row and those using the WAsP recommended value closer to the data for the first turbines. It is generally seen that under stable and unstable atmospheric conditions the power deficits are the highest and lowest, respectively, but the wind conditions under both stability regimes are different. The ensemble average of the simulations does not approach the limits of the infinite wind farm under any stability condition as such averages account for directions misaligned with the row.

© 2014 Elsevier Ltd. All rights reserved.

1. Introduction

In the last years, investigation of the effect of atmospheric stability on the production of wind farms has gained attention, partly because it has been observed, particularly at large offshore wind farms, that under stable and unstable atmospheric conditions, the wind farms under- and over-perform, respectively, when compared to wind farm data under neutral conditions [6]. Most wake models do not account for stability conditions other than neutral and, thus, model under-performance – when compared to wind farm data – is sometimes attributed to the effect of atmospheric stability.

The Park wake model [8] used in the Wind Atlas Analysis and Application Program (WAsP) [9] is based on the model of Ref. [7], which makes use of the wake decay coefficient k_w to estimate the wind speed reduction for a given thrust coefficient, downstream distance, turbine diameter, and upstream wind speed. It is recommended in WAsP to use $k_w = 0.05$ for offshore wind farms (lower than the recommended value onshore of 0.075). This is because k_w is related to the entrainment of the wake in the atmosphere (it is in fact the slope of the expansion of the wake) and as such it is a function of the surface roughness z_o (the lower the roughness the less wake expansion). Ref. [2], by semi-empirical means, suggested $k_w = 0.5/\ln(h/z_o)$, where h is the turbine's hub height, which generally translates into lower k_w-values than the WAsP recommendations (e.g. Frandsen's k_w becomes 0.039 for a typical wind turbine offshore). Ref. [1] found that using $k_w = 0.03$ adjusted well the results of the Park wake model at the Nysted wind farm when compared to data. Interestingly, at Nysted, i.e. in the South Baltic Sea, stable conditions are mostly observed, whereas at Horns Rev I (a wind farm in the North Sea, where the conditions are generally less stable than at Nysted) good model performance has been found with a slightly higher k_w-value [3].

Here, we present an analysis of wind farm data carried out at the Horns Rev I wind farm, where we are able to classify wind turbine power data into different atmospheric stability classes. A large set of simulations using a modified version of the Park wake model are performed using different k_w-values correspondent to particular atmospheric stability conditions. The simulations are post-processed in order to partly take into account the wind direction uncertainty and compared to the data. Since Horns Rev I is a rather large wind farm, for the wind directions analyzed we might expect that some cases will approach the limits of an infinite wind farm. Therefore, we also present the results of the Park wake model evaluated to its infinite theoretical limits.

* Corresponding author. Tel.: +45 23676361.
E-mail addresses: aldi@dtu.dk (A. Peña), pire@dtu.dk (P.-E. Réthoré), olra@dtu.dk (O. Rathmann).

http://dx.doi.org/10.1016/j.renene.2014.02.019
0960-1481/© 2014 Elsevier Ltd. All rights reserved.

Please cite this article in press as: Peña A, et al., Modeling large offshore wind farms under different atmospheric stability regimes with the Park wake model, Renewable Energy (2014), http://dx.doi.org/10.1016/j.renene.2014.02.019

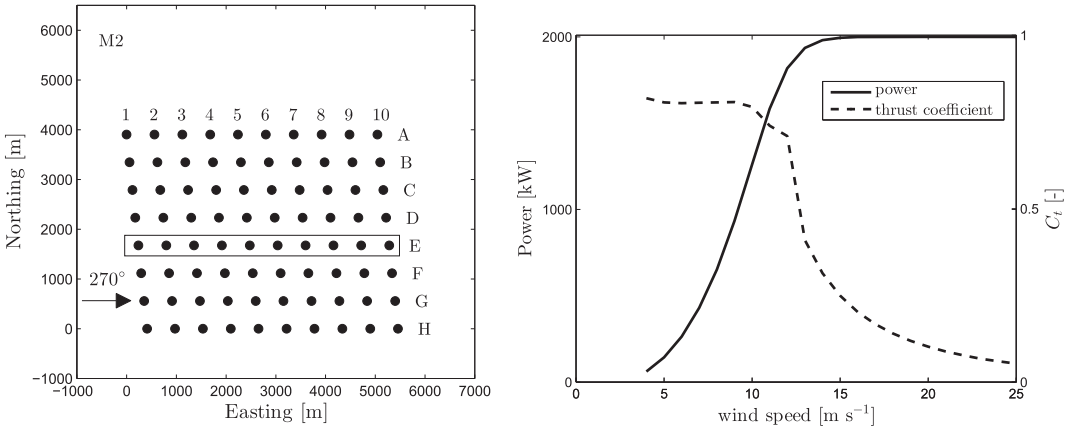

Fig. 1. (Left) The Horns Rev I offshore wind farm and the location of the met mast (M2). Row E (used in this study) is framed. (Right) Power and thrust coefficient (C_t) as a function of wind speed for the Vestas V80 wind turbine.

2. Modified Park wake model

We implemented the Park wake model described in Ref. [8] in a Matlab script to run simulations for a wide variety of wind directions, wind speeds, wind farm layouts, wind turbine specifications, and k_w-values. We refer to it as "modified" because in WAsP the model has been extended to account for the effect of ground-reflected wakes from upwind turbines and our version takes into account the wakes upwind (directly or sideways) only. Partial wakes (from misalignments between the local and the upstream turbines' direction and the wind direction itself) are treated as in Ref. [17], i.e. the local velocity is reduced by a factor depending on the turbine and the wake geometry. Ref. [15] illustrated the modified Park wake model in detail, its approach to account for merging wakes, and the effect of partial wakes.

Ref. [14] showed that adjusting k_w to match the wind speed reductions estimated by a stability-dependent infinite wind-farm boundary-layer model (a totally different model based on the concept of [2], which generally gives higher wind speed reductions in stable compared to unstable conditions) resulted in lower k_w-values under stable compared to unstable conditions. The adjustment was performed evaluating the Park wake model for an infinite wind farm. Similar results were found when evaluating this 'infinite' Park wake (IPW) model assuming,

$$k_w \approx u_{*\mathrm{free}}/u_{\mathrm{hfree}} \approx \kappa/[\ln(h/z_o) - \psi_m(h/L)], \tag{1}$$

where $u_{*\mathrm{free}}$ and u_{hfree} are the undisturbed friction velocity and hub-height wind speed, respectively, $\kappa = 0.4$ is the von Kármán constant, and $\psi_m(h/L)$ is the extension to the logarithmic wind profile to account for stability and depends on the height (in this case the hub-height) and atmospheric stability by means of L (the Obukhov length). The expressions for ψ_m can be found in Ref. [10]. Since our Matlab implementation only accounts for upwind wakes, we use the IPW model expressions for the same type of wakes,

$$\delta_I^2 = \frac{\mathrm{psi}\left[3, 1 + (2s_r k_w)^{-1}\right]}{96 s_r^4 k_w^4}, \tag{2}$$

$$\delta_{III}^2 = \frac{-0.0625\,\mathrm{psi}\left[2, s_f/(s_r k_w)\right]}{s_f s_r^3 k_w^3}, \tag{3}$$

where δ_I^2 and δ_{III}^2 are the contributions of the wakes directly upwind and upwind partial wakes, respectively, and s_r and s_f are the along- and cross-wind turbine to turbine distances non-dimensionalized by the turbine diameter. The 'infinite' limit thus becomes,

$$\frac{u_\infty}{u_{\mathrm{free}}} = 1 - e_o\left(\delta_I^2 + \delta_{III}^2\right)^{1/2}, \tag{4}$$

where u_∞ is the wind speed upstream the last turbine in the infinite wind farm, u_{free} the undisturbed wind speed, and $e_o = 1 - (1 - C_t)^{1/2}$, being C_t the thrust coefficient (so it is assumed that this is constant throughout the wind farm). The details of the derivation of the above three equations are given in Ref. [14].

3. Horns Rev I wind farm

The Horns Rev I wind farm is located in the Danish North Sea at about 17 km west from the coast (from the wind farm's northwest corner). A layout of the wind farm showing the positions of the 80 wind turbines (rows are named from A to H and columns from 1 to 10) and a meteorological (met) mast are shown in Fig. 1-left. The turbines are Vestas V80 2 MW machines of 80-m rotor diameter and 70-m hub height. Power and thrust-coefficient curves are illustrated in Fig. 1-right.

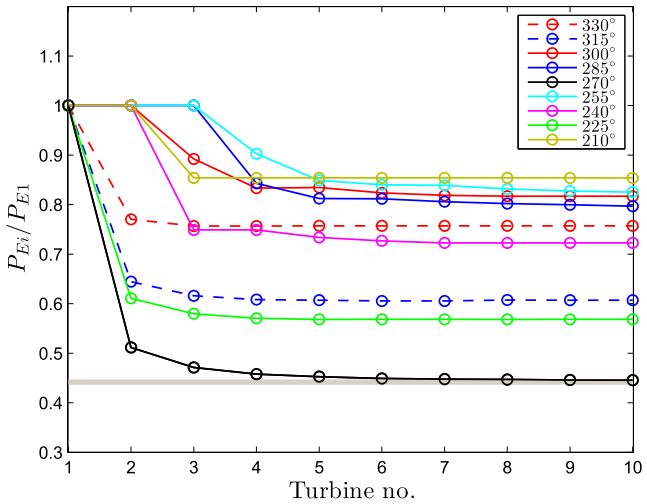

Fig. 2. Simulated power deficits of row E (normalized with the power of turbine 05 P_{E1}) for different westerly directions with $k_w = 0.05$. The thick gray solid line indicates the infinite wind farm limit.

Please cite this article in press as: Peña A, et al., Modeling large offshore wind farms under different atmospheric stability regimes with the Park wake model, Renewable Energy (2014), http://dx.doi.org/10.1016/j.renene.2014.02.019

The met mast (M2) is located about 2 km north from the northwest edge of the wind farm. Met data from this mast have been extensively analyzed for atmospheric stability studies (e.g. in Refs. [11–13]). Here we use measurements from the cup anemometers at 62 and 15 m above mean sea level (AMSL—all measurements are referred to AMSL hereafter unless otherwise stated), a wind vane at 43 m, temperature sensors at 13 and −4 m (the latter is below mean sea level), and humidity and pressure sensors at 13 and 55 m, respectively.

3.1. Power deficit sensitivity to wind direction

Before comparing the model simulations with wind farm data, the sensitivity of the power deficit to the wind direction at Horns Rev I can already be analyzed from the simulations alone. As we will focus the data analysis on row E and westerly winds, Fig. 2 illustrates the simulated power deficits at that row for wind directions in the range 210°–330° with $u_{\mathrm{hfree}} = 8.5$ m s^{-1}. The simulations are performed with the modified Park wake model using the recommended WAsP k_{w}-value offshore and are not post-processed to partly account for the direction uncertainty because 1) the latter weights simulations over a range of directions other than that from which the analysis is performed and 2) the infinite wind farm limit on this row might be reached at 270° as this direction is aligned with the row direction; this limit is estimated using Eq. (4) with $s_{\mathrm{r}} = s_{\mathrm{f}} = 7$ (from the geometry of the wind farm), $k_{\mathrm{w}} = 0.05$, and C_{t} derived from u_{hfree} using the thrust curve.

As expected the highest power deficits are simulated at 270° (as the wakes are directly superposed) and this is the only westerly direction in which the infinite limit is reached, already at about the fifth turbine (when accounting for direction uncertainty the limit is not longer reached as directions other than 270° are also taken into account). The directions 255° and 285° show some of the lowest power deficits (turbines E2 and E3 are not wake affected) and only turbine E4 at those directions is affected by the wake of turbines F1 and D1, respectively. Interestingly, the directions 225° and 315° show the second highest power deficits as for both cases turbine E2 is nearly directly downstream turbines F1 and D1, respectively.

4. Data treatment

Concurrent 10-min data from the wind turbines and M2 between January 1, 2003 and December 31, 2008 are used. Data from the turbines include a power quality signal indicating the status of the turbine and the power signal (stopped, down-regulated, etc.). We choose to use data when all turbines show status equal to 1, i.e. a validated measurement where the turbine does not stop and there are no spikes or drop outs in the power signal; such data are found only after February 7, 2005 in our database.

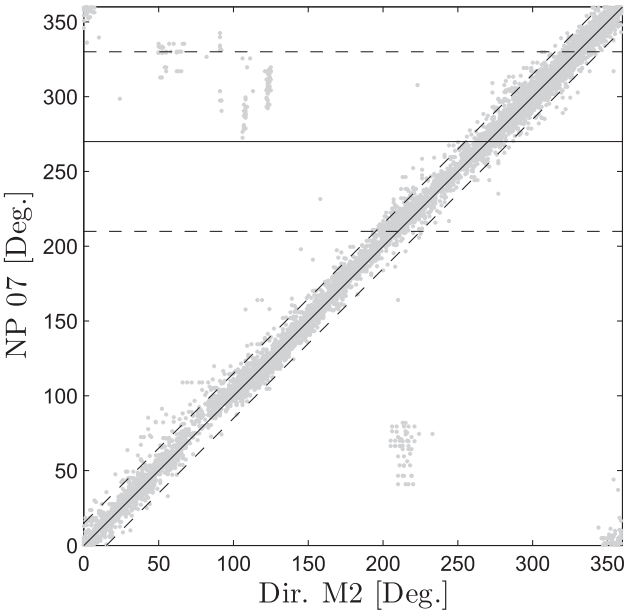

Fig. 3. Wind direction observed at M2 at 43 m and the nacelle position (NP) of turbine 07 (G1). The lines illustrate the filtering criteria used for the data (see text for details).

Atmospheric stability at the wind farm is assessed using the observations from M2. In order to filter data where the climate/conditions are not similar at the two places, we first analyze the wind direction observed at M2 and that at turbine 07 (row G, column 1). For the latter we use the nacelle position, which was found to be optimal for analyzing the wake effect for wind directions 270 ± 60° [5]. Fig. 3 shows a scatter plot between the two measurements where it is observed a very good correspondence for most cases. We select cases where the difference between both signals is lower than 15° and where the wind direction at turbine 07 (G1) is 270 ± 60° (the latter criterion also ensures that no wakes affect the stability estimations at M2 and might allow us to study the array in the limits of the infinite wind farm).

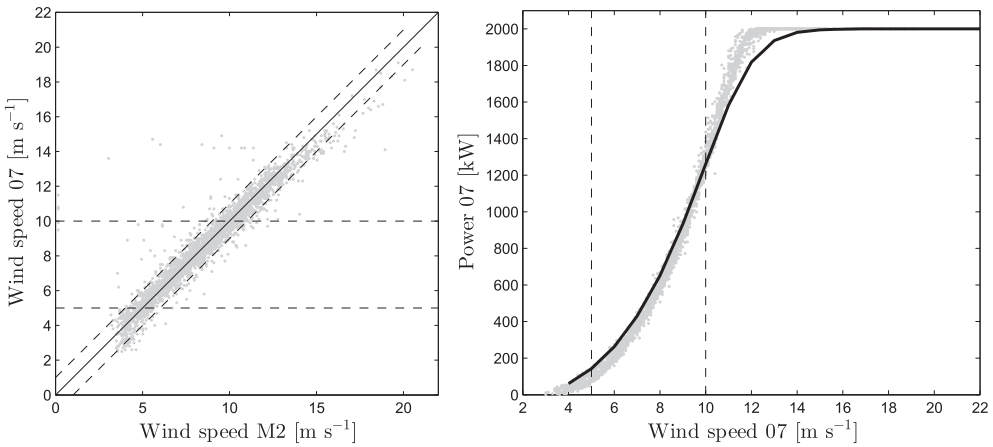

Fig. 4. (Left) Comparison of the wind speeds observed at M2 at 62 m with those at the nacelle of turbine 07 (G1) at 70 m. The lines illustrate the filtering criteria used for the data (see text). (Right) Power performance at turbine 07 (G1) based on its nacelle wind speed. The solid line shows the power curve used in this study.

Please cite this article in press as: Peña A, et al., Modeling large offshore wind farms under different atmospheric stability regimes with the Park wake model, Renewable Energy (2014), http://dx.doi.org/10.1016/j.renene.2014.02.019

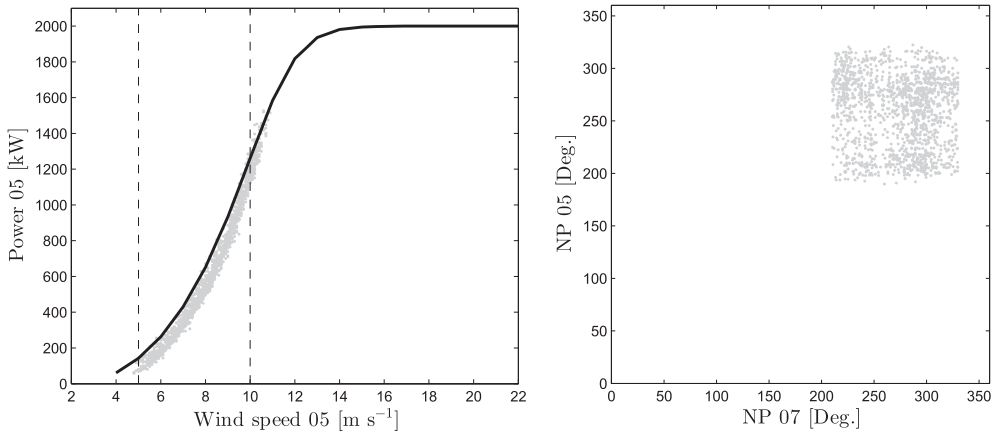

Fig. 5. (Left) As Fig. 4-right but for turbine 05 (E1). (Right) Comparison of the nacelle position signals of turbines 05 (E1) and 07 (G1).

We further study the agreement between the wind speeds observed at M2 at 62 m and the nacelle ones at turbine 07 (G1) at 70 m (Fig. 4-left). As illustrated both signals show very good agreement and so we use them to further filter data: we choose the wind speed range 5–10 m s^{-1} (since the thrust coefficient is nearly constant within this range) and the difference between both signals needs to be lower than 1 m s^{-1}. Before this 'filtering' step, we check the power performance using the wind speed and power signals of turbine 07 (G1), which as seen in Fig. 4 compares well with the one provided by the manufacturer (slightly over- and under-estimating the power below and above ~10 m s^{-1}, respectively).

Our analysis is focused on the wind speed deficits of row E (see Fig. 3) and so we extract power data correspondent to the turbines on that row only. We use another filtering criterion based on the standard deviation of the power signal. It is noted a good amount of data with negative power values and we were advised to use values higher than 5 kW for the standard deviation of the power for the analysis (Kurt Hansen, personal communication) as this indicates that the turbine might be operating in a transition mode. We increase the criterion to 12 kW. This reduced dataset is then complemented with the nacelle position and wind speed of turbine 05 (row E, column 1) and the measurements from M2. Atmospheric static stability is derived by estimating the bulk Richardson number $\mathrm{Ri_b}$ as

$$\mathrm{Ri_b} = -\frac{gz\Delta\theta_v}{\overline{T}\overline{U}^2}, \tag{5}$$

where g is the Earth's gravitational acceleration, z is the height where the observations of mean temperature $\overline{T}$ and wind speed $\overline{U}$ are taken (in this case 15 and 13 m, respectively), and $\Delta\theta_v$ is the difference between the virtual potential temperatures at the surface and the height z (in this case −4 and 13 m, respectively; see Ref. [13] for details). Estimations of the dimensionless stability parameter z/L are based on $\mathrm{Ri_b}$ depending on the stability condition. For unstable and stable conditions, these are, respectively:

$$\frac{z}{L} = C_1\mathrm{Ri_b}, \tag{6}$$

$$\frac{z}{L} = \frac{C_1\mathrm{Ri_b}}{1 - C_2\mathrm{Ri_b}}, \tag{7}$$

where $C_1 \approx 10$ and $C_2 \approx 5$ implying a critical $\mathrm{Ri_b} = 0.2$ [4].

Fig. 5-left shows the power performance of turbine 05 (E1), where a very similar behavior to that observed for turbine 07 (G1) is found (Fig. 4-left). For the rest of the analysis, we use the wind speed resulting from converting the power to wind speed of turbine 05 (E1) (through the power curve in Fig. 1-right) as a proxy for the undisturbed wind speed. For completeness, we illustrate in Fig. 5-right that the nacelle position of turbine 05 (E1) cannot be used for wake analysis since it is rather different to that of turbine 07 (G1).

5. Results

The nearly final dataset results in 1525 10-min values (Table 1 shows the amount of 10-min observations after each filtering step). The data is classified in four stability classes: very unstable ($-1.5 \le z/L \le -0.2$), unstable ($-0.2 \le z/L \le -0.03$), neutral ($|z/L| \le 0.03$), and stable ($3 \ge z/L \ge 0.03$) with z=15 m. Fig. 6-left shows the ensemble average of power deficits of row E (normalized with the power of turbine 05 (E1)) for the different stability classes. Although it is observed a general higher power reduction in stable compared to unstable conditions, this type of comparison is misleading, since the wind speed and direction conditions under each stability class are not the same. Fig. 6-right illustrates the histograms of wind speed for the different stability conditions and is noticed that they show different distributions. We further narrow the analysis to wind speeds within the range 8.5 ± 0.5 m s^{-1} to reduce the variability of wind conditions maximizing the amount of data.

Although the reduction in the variability of power deficits, for each stability class the difference in the individual 10-min power deficit values is very large. One of the main reasons for this is that the observed wind direction range is rather broad and the direction distributions are different (Fig. 7). However we cannot narrow the range any further as we might find very few or no data: e.g. very unstable and unstable conditions are mostly seen within the range 290°–310°, whereas there are no data and only few of them for that range under neutral and stable conditions, respectively.

Table 1
Amount of 10-min periods left for wake analysis after the filtering criteria applied to the Horns Rev I dataset (see text in the Data treatment section for details).

No. of 10-min	Description of filtering
315,648	Original available database from 2003 to 2008
11,513	All 80 turbines show power signal status equal to 1
2850	$\mathrm{DIR_{G1}} = 270 \pm 60°$ and $\lvert\mathrm{DIR_{G1}} - \mathrm{DIR_{M2}}\rvert \le 15°$
1525	$u_{G1} = 5$–10 m s^{-1}, $\lvert u_{G1} - u_{M2}\rvert \le 1$ m s^{-1}, $\sigma_{P_E} > 12$ k_w
308	$u_{E1} = 8.5 \pm 0.5$ m s^{-1}

Please cite this article in press as: Peña A, et al., Modeling large offshore wind farms under different atmospheric stability regimes with the Park wake model, Renewable Energy (2014), http://dx.doi.org/10.1016/j.renene.2014.02.019

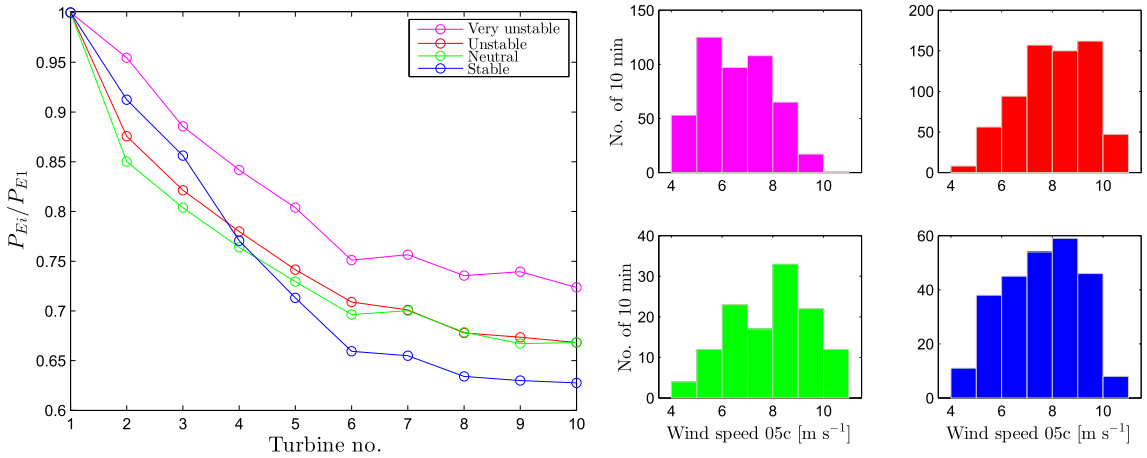

Fig. 6. (Left) Ensemble average power deficit of row E (normalized with the power of turbine 05 P_{E1}) for different atmospheric stability conditions. (Right) Wind speed histograms (based on the power-converted value from turbine 05 (E1)) for each stability condition.

For each stability class we choose to run simulations using the Horns Rev I layout (thrust coefficient and power curves as in Fig. 1) with the modified Park wake model for $u_{\mathrm{hfree}} = 8.5$ m s^{-1} and a wide undisturbed wind direction range of 180°–360° (at a resolution of 0.5°; nearly identical results are found for a resolution of 0.1°). This is performed for k_{w}-values of 0.05, 0.0349, 0.0338, 0.0313, and 0.0231, which correspond, respectively, to the WAsP recommended one, and those for very unstable, unstable, neutral, and stable conditions. For the estimation of these stability-dependent k_{w}-values, we average the bulk Richardson number from Eq. (5) under each stability class, convert this average estimation into a z/L value using either Eq. (6) or (7), estimate the ψ_{m} correction at hub height, and evaluate Eq. (1) assuming $z_{\mathrm{o}} = 0.0002$ m.

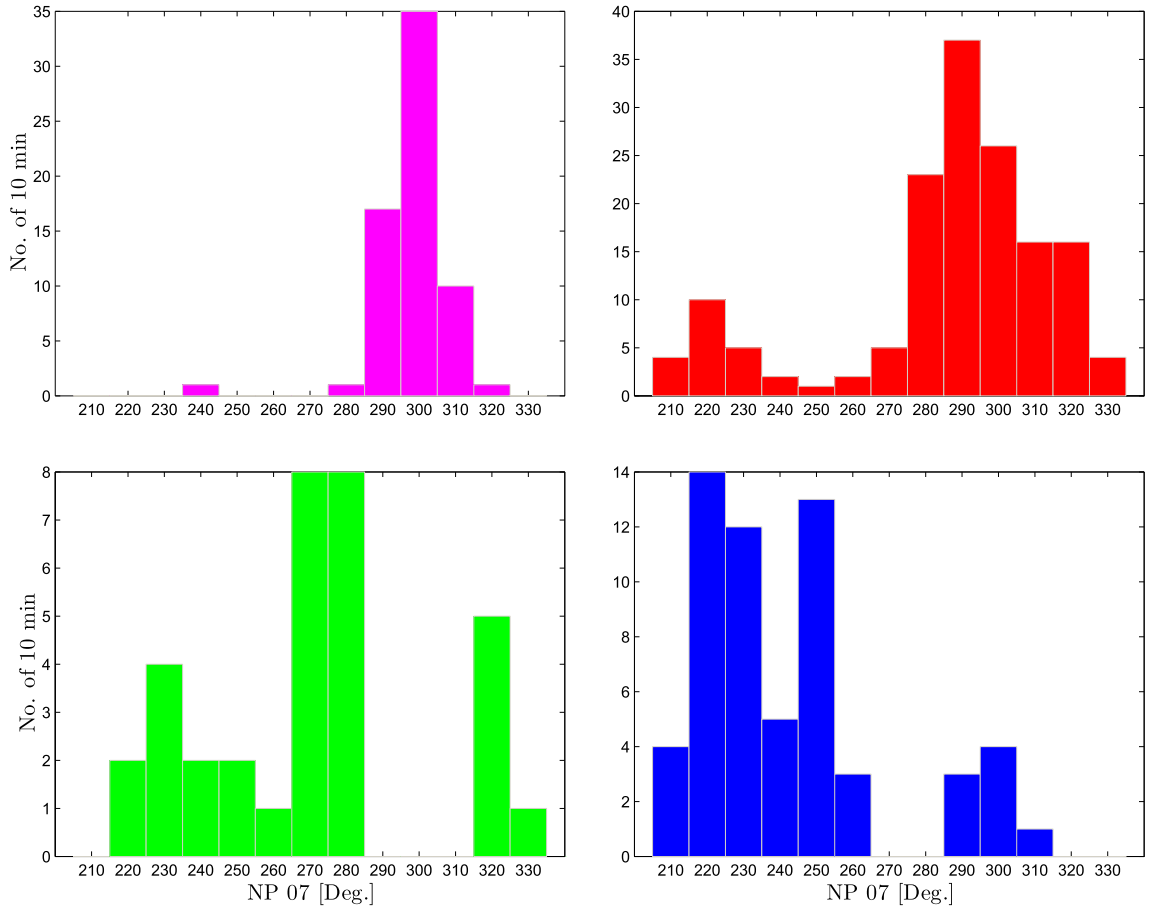

Fig. 7. Wind direction histograms (based on the nacelle position of turbine 07 (G1)) for each stability condition: very unstable (top left), unstable (top right), neutral (bottom left), and stable (bottom right).

Please cite this article in press as: Peña A, et al., Modeling large offshore wind farms under different atmospheric stability regimes with the Park wake model, Renewable Energy (2014), http://dx.doi.org/10.1016/j.renene.2014.02.019

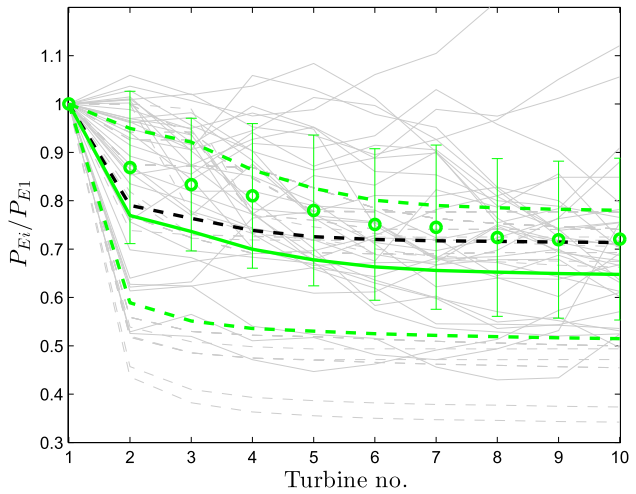

Fig. 8. Power deficits of row E (normalized with the power of turbine 05 P_{E1}) for neutral conditions. The gray solid lines show the 10-min observed power deficits (in gray dashed lines for each simulation), the colored circles the ensemble average of observations (error bars with ± the standard deviation), the solid colored line the ensemble average of the simulations with the stability-specific k_w-value (dashed colored lines indicate the ±standard deviation), and the black dashed line the ensemble average of the simulations with $k_w = 0.05$. (For interpretation of the references to color in this figure legend, the reader is referred to the web version of this article.)

The simulations are further post-processed to take into account part of the wind direction uncertainty as in Refs. [3,15], i.e. assuming that within a 10-min interval the wind direction distributes as a normal distribution with a given standard deviation σ. We use a value of 2.5° based on the analysis by Ref. [3] of sonic high frequency observations of wind direction at Horns Rev, which are not available for the period used in our analysis. The procedure is briefly as follows: for each observed 10-min wind direction θ under each atmospheric stability class, we extract the simulations correspondent to the range $\theta \pm 3\sigma$. We then weight each simulation using the normal probability distribution function. For each observed 10-min wind direction and speed deficit, there is therefore a single simulated wind speed deficit (derived from 31 Gaussian-weighted simulations).

Figs. 8–11 show the results of the comparison of the observed 10-min power deficits and those simulated at row E for the different stability classes. They are not shown in the same figure as they correspond to observations/simulations under different wind direction conditions. The ensemble average of both simulations (with a stability-specific k_w-value) and observations are also shown together with that of the simulations using $k_w = 0.05$. As the results of the simulations are wind speed deficits, we translate them into power deficits with the power curve in Fig. 1.

The results generally show a good agreement between the ensemble averages of simulations and observations. For each stability condition the result using the stability-specific k_w-value shows higher power reductions compared to that using $k_w = 0.05$, as a lower k_w-value increases the wake effect. Particularly, under neutral stability conditions, the ensemble average of the simulations using both the stability-specific and WAsP recommended k_w-values shows that the model predict higher power deficits than observed for all turbines in the row. This is very interesting because in many studies at Horns Rev I and at other large offshore wind farms where the Park wake model has been used, the results are sometimes the opposite: model underprediction of the power/speed deficits [1,16]. This might be partly due to the range of wind directions we use for our analysis and to the post-processing of the simulations accounting for the wind direction uncertainty.

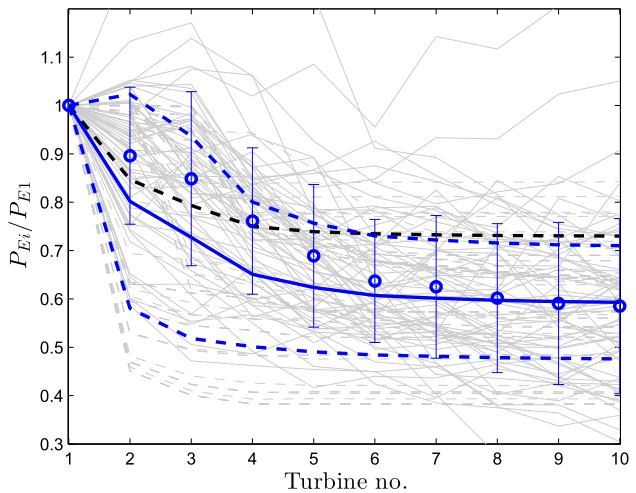

Fig. 9. As Fig. 8 but for stable conditions.

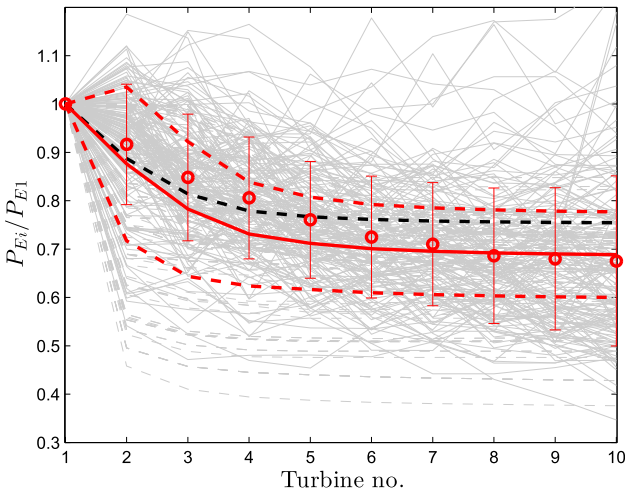

Fig. 10. As Fig. 8 but for unstable conditions.

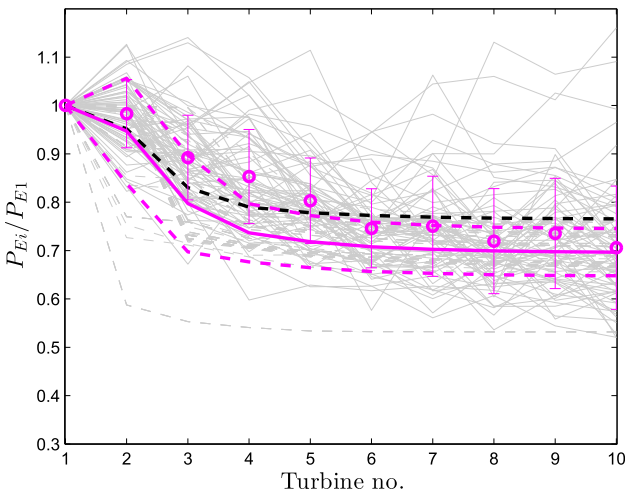

Fig. 11. As Fig. 8 but for very unstable conditions.

Please cite this article in press as: Peña A, et al., Modeling large offshore wind farms under different atmospheric stability regimes with the Park wake model, Renewable Energy (2014), http://dx.doi.org/10.1016/j.renene.2014.02.019

Table 2
Root mean square error from the observed and simulated ensemble averages of normalized power deficits for row E for each stability condition and type of simulation (k_w- and σ-dependent).

Type of simulation	Neutral	Stable	Unstable	Very unstable
Stability-dependent k_w				
$\sigma = 2.5^\circ$	0.090	0.068	0.041	0.064
$\sigma = 5.0^\circ$	0.113	0.061	0.047	0.060
WAsP k_w				
$\sigma = 2.5^\circ$	0.048	0.098	0.051	0.044
$\sigma = 5.0^\circ$	0.054	0.105	0.049	0.044

Apart from the neutral case (which is the one with the least data), the simulation with the stability-dependent k_w fits better the power deficit at the last turbines in the row compared to the simulations using $k_w = 0.05$, which in turn generally fit well the results of the first turbines in the row. However, most of the outliers (i.e. the individual observed 10-min power deficits where $P_{Ei}/P_{E1} > 1$) are found at those first turbines in the row (there are fewer outliers at the last turbines). Removing such 'outliers' brings the ensemble average of observations closer to that of the simulations but there are no reasons to remove them as there are no other available signals indicating the malfunctioning of any sensor.

We can also note that the range of the results of the simulations and that of the observations for each stability class is well predicted (except for the clear outliers). The cloud of observations (and simulations) of power deficits for unstable conditions is clearly between 0.5 and 0.8 and for very unstable conditions between 0.6 and 0.8. The uncertainty of the observations and the simulations (given by the standard deviation as shown in the figures) is rather similar for all stability conditions and wake-affected turbines (E2–E10). However, the uncertainty of observations tends to be higher in the last turbine (E10), whereas it is generally higher at the second one (E2) for the simulations.

The largest power deficit drop is observed at turbine E2 (as expected from the sensitivity analysis in Section 3.1) and appears in the neutral class (this is the one where most of the observed wind comes from 270°). Under the stable class we can also observe a high drop in power deficit for turbine E2; most of the wind for this class comes from 220° and as shown in Fig. 2 for that wind direction, turbine F1 is directly upstream E2.

The infinite limits of power reduction are 0.26, 0.15, 0.28, 0.30, and 0.44 for neutral, stable, unstable, very unstable, and the WAsP-recommended k_w-values, respectively. None of the ensemble averages of simulated or observed power deficits approach the limits as they account for directions other than 270°.

Also interestingly, under very unstable atmospheric conditions the ensemble average of observed power deficit at turbine E2 is very similar to that at turbine E1; as shown in Fig. 7 for this atmospheric stability condition, winds parallel to the row are not observed and winds mostly come from 300°. Fig. 2 shows that for that particular direction, turbine E1 does not shade any turbine on row E. Turbine E2 is thus mostly affected by partial wakes from turbine D1 (if any).

Table 2 illustrates the summary of the performance of the modified Park wake model when compared to the observations including the post-processing for partly accounting for the direction uncertainty. Results using the stability-dependent k_w-values and the WAsP recommended one as well as for two σ-values are given. Generally, the performance of the model does not significantly change for varying σ-values as the simulations are performed over a wide range of directions; for the WAsP-k_w the results using $\sigma = 2.5^\circ$ are better for all stability conditions (except unstable). The highest changes in performance are found when varying k_w; however the most suitable type of k_w-value depends on the atmospheric condition.

6. Conclusions and discussion

Power deficit data from the Horns Rev I offshore wind farm are analyzed under different atmospheric stability conditions, a nearly constant undisturbed wind speed, and a wide range of westerly wind directions. The resulting dataset is compared with simulations using a modified version of the Park wake model and the limits of the Park wake model when evaluated as an infinite wind farm.

It is found a good agreement between simulations and observations for a west-east row in the middle of the wind farm. The simulations using a stability-dependent k_w-value are closer to the observations at the last turbines and those using the WAsP recommended k_w-value of 0.05 closer to the observations at the first turbines on that row.

Due to the range of observed and simulated wind directions, it is difficult to conclude whether under stable or unstable atmospheric conditions the wind farm, respectively, under- or over-performs. However, it is seen higher power reductions under stable than unstable atmospheric conditions. In none of the conditions, the observations seem to approach the limits of the infinite wind farm.

It is important to mention that by filtering data, where the conditions at the mast and those at the wind turbine row are similar (as stability can only be derived at the mast) the results of our analysis are valid for a specific set of conditions, which might be rarely observed. The mast is more than 4 km from the row and wind speed, wind direction, and stability normally vary within the area of analysis.

Here, we focus the analysis on a value of 2.5° for the standard deviation of the direction within a 10-min interval based on the observations of [3], who found a similar value when analyzing sonic measurements at M2 for a westerly direction. The uncertainty of the direction will be generally higher than the variability of the natural variation of the wind direction and so simulations performed with a higher σ-value will generally show a higher power ratio. However, the ideal scenario is to measure such variability and uncertainty for each 10-min period and perform the post-processing accordingly.

Stability through the wind farm is here assumed to be constant. We expect that the local stability varies downstream the wind farm and so the wake decay coefficient and uncertainty. However, there are few studies analyzing the changes in momentum and heat flux within the wind farm and they show opposite trends [14] (they are based on numerical computations or wind tunnel studies not on atmospheric observations).

Acknowledgments

We would like to thank funding from the EERA DTOC project (FP7-ENERGY-2011-1/nr.282797) and from the IEA-WakeBench collaboration initiative. Horns Rev data were kindly provided by Vatenfall A/S and DONG Energy A/S.

References

[1] Barthelmie R, Jensen LE. Evaluation of wind farm efficiency and wind turbine wakes at the Nysted offshore wind farm. Wind Energy 2010;13:573–86.
[2] Frandsen S. On the wind speed reduction in the center of large clusters of wind turbines. J Wind Eng Ind Aerodyn 1992;39:251–65.
[3] Gaumond M, Rethoré PE, Ott S, Peña A, Bechmann A, Hansen KS. Evaluation of the wind direction uncertainty and its impact on wake modelling at the horns rev offshore wind farm. Wind Energy; 2013 [in press].
[4] Grachev AA, Fairall CW. Dependence of the Monin-Obukhov stability parameter on the bulk Richardson number over the ocean. J Appl Meteorol 1996;36:406–14.

Please cite this article in press as: Peña A, et al., Modeling large offshore wind farms under different atmospheric stability regimes with the Park wake model, Renewable Energy (2014), http://dx.doi.org/10.1016/j.renene.2014.02.019

ARTICLE IN PRESS

[5] Hansen KS, Barthelmie RJ, Jensen LE, Sommer A. The impact of turbulent intensity and atmospheric stability on power deficits due to wind turbine wakes at horns rev wind farm. Wind Energy 2012;15:183–96.
[6] Jensen LE. Array efficiency at Horns Rev and the effect of atmospheric stability. In: Proceedings of the European wind energy association conference & exhibition, Milano; 2007.
[7] Jensen NO. A note on wind generator interaction. Technical Report Risoe-M-2411(EN). Roskilde: Risø National Laboratory; 1983.
[8] Katic I, Højstrup J, Jensen NO. A simple model for cluster efficiency. In: Proceedings of the European wind energy association conference & exhibition, Rome; 1986.
[9] Mortensen NG, Heathfield DN, Myllerup L, Landberg L, Rathmann O. Getting started with WAsP 9. Technical Report Risø-I-2571(EN). Roskilde: Risø National Laboratory; 2007.
[10] Peña A. Sensing the wind profile. Technical Report Risø-PhD-45(EN). Roskilde: Risø DTU; 2009.
[11] Peña A, Gryning SE. Charnock's roughness length model and non-dimensional wind profiles over the sea. Bound Layer Meteorol 2008;128:191–203.
[12] Peña A, Gryning SE, Hasager CB. Measurements and modelling of the wind speed profile in the marine atmospheric boundary layer. Bound Layer Meteorol 2008;129:479–95.
[13] Peña A, Hahmann AN. Atmospheric stability and turbulent fluxes at Horns Rev – an intercomparison of sonic, bulk and WRF model data. Wind Energy 2012;15:717–30.
[14] Peña A, Rathmann O. Atmospheric stability-dependent infinite wind-farm models and the wake-decay coefficient. Wind Energy; 2013 [in press].
[15] Peña A, Réthoré P.-E, Hasager C.B, Hansen K.S. Results of wake simulations at the Horns Rev I and Lillgrund wind farms using the modified Park model, Technical Report, DTU Wind Energy-E-Report 0026(EN), 2013, Roskilde
[16] Rathmann OS, Frandsen S, Nielsen M. Wake decay constant for the infinite wind turbine array. In: Proceedings of the European wind energy association conference & exhibition, Warsaw; 2010.
[17] Wan C, Wang J, Yang G, Gu H, Zhang X. Wind farm micro-siting by Gaussian particle swarm optimization with local search strategy. Renew Energy 2012;48:276–86.

Please cite this article in press as: Peña A, et al., Modeling large offshore wind farms under different atmospheric stability regimes with the Park wake model, Renewable Energy (2014), http://dx.doi.org/10.1016/j.renene.2014.02.019